Coupling between Buoyancy Forces and Electroconvective Instability near Ion-Selective Surfaces

Elif Karatay,[1,*] Mathias Bækbo Andersen,[1] Matthias Wessling,[2] and Ali Mani[1,†]
[1]Department of Mechanical Engineering, Stanford University and Center for Turbulence Research, Stanford University, Stanford, California 94305, USA
[2]RWTH Aachen University, Aachener Verfahrenstechnik, 52056 Aachen, Germany
(Received 16 October 2015; published 12 May 2016)

Recent investigations have revealed that ion transport from aqueous electrolytes to ion-selective surfaces is subject to electroconvective instability that stems from coupling of hydrodynamics with electrostatic forces. These systems inherently involve fluid density variation set by salinity gradients. However, the coupling between the buoyancy effects and electroconvective instability has not yet been investigated although a wide range of electrochemical systems are naturally prone to these interplaying effects. In this study we thoroughly examine the interplay of gravitational convection and chaotic electroconvection. Our results reveal that buoyant forces can significantly influence the transport rates, otherwise set by electroconvection, when the Rayleigh number Ra of the system exceeds a value $\mathrm{Ra} \sim 1000$. We show that buoyancy forces can significantly alter the flow patterns in these systems. When the buoyancy acts in the stabilizing direction, it limits the extent of penetration of electroconvection, but without eliminating it. When the buoyancy destabilizes the flow, it alters the electroconvective patterns by introducing upward and downward fingers of respectively light and heavy fluids.

DOI: 10.1103/PhysRevLett.116.194501

Mass transfer beyond diffusion limitation is possible in electrically driven systems when ions are transported from a fluid electrolyte to a charge-selective interface, e.g., an ion exchange membrane or an electrode. Among several mechanisms on the origins of this overlimiting mass transfer, electroconvection, which is an instability arising from coupling between flow and ion transport via electrostatic effects, has been suggested as one of the key mechanisms [1]. In such systems when the applied voltage is above a threshold (for example, $\gtrsim$0.5 V for aqueous systems with monovalent ions at room temperature), oscillations in the instantaneous current signal have been measured while an overlimiting current is sustained [2,3]. The noise in the electric response has been attributed to induced convection [2–6], and indeed flow vortices have been observed in experiments [7–9]. Consistent with these observations, a theoretical analysis has shown that ion transport across charge-selective interfaces is prone to electrokinetic instabilities (EKIs) stemming from a coupling of the fluid flow with ion transport and electrostatic interactions [10]. More recent direct numerical simulations demonstrated transitions from regular coherent vortices to chaotic multiscale structures when the applied potential is higher than a limit ($\gtrsim$1 V) [11–14]. In all these studies, however, gravitational effects have been neglected.

Systems prone to EKI experience fluid density gradients even before the onset of EKI due to strong salt concentration gradients associated with the ion-concentration polarization phenomenon [10,15]. Previous studies have considered gravitational effects in electrochemical systems but ignored electrokinetic effects. The requirements for the onset of gravitational instabilities are often satisfied when the Rayleigh number $\mathrm{Ra} = \beta \Delta c g L^3/\nu D$ of the system exceeds a critical value in electrolytic systems [2–6,15–24]. Here, L is the distance from bottom to top boundary, g is the magnitude of the gravitational acceleration, β and D are the solute expansion coefficient and diffusivity of the electrolyte, ν is the kinematic viscosity of the fluid, and Δc represents the scale for the variation in the concentration. Provided that the Ra number is sufficiently large in a gravitationally unstable arrangement [Fig. 1(a)], flow vortices arise due to the action of buoyant forces. Buoyant flow structures have been experimentally observed near ion-selective interfaces [21,25–27]. Their significant impact on the limiting current i_{lim} [4,5,18–20,28,29] and the morphology of the electrodeposits [25,27,30,31] have been reported in low voltage range experiments for decades. In fact, electrochemical experiments have been used as a surrogate to model the buoyancy-driven flow in the Rayleigh-Bénard (RB) convection problem [20,21,29]. Most of these experiments were set at voltages close to the onset of limiting current to achieve $c \approx 0$ close to the ion-absorbing boundary and thus ensure a well-defined Rayleigh number [21,22,29,32]. This regime happens to be well below the threshold for EKI effects. However, most practical scenarios in various electrochemical applications such as electrodeposition, electroplating, and electrodialysis [9,30,33] involve regimes where the applied voltage and system Rayleigh number are both above their critical values and thus inevitably involve coupling of electroconvection with buoyancy effects.

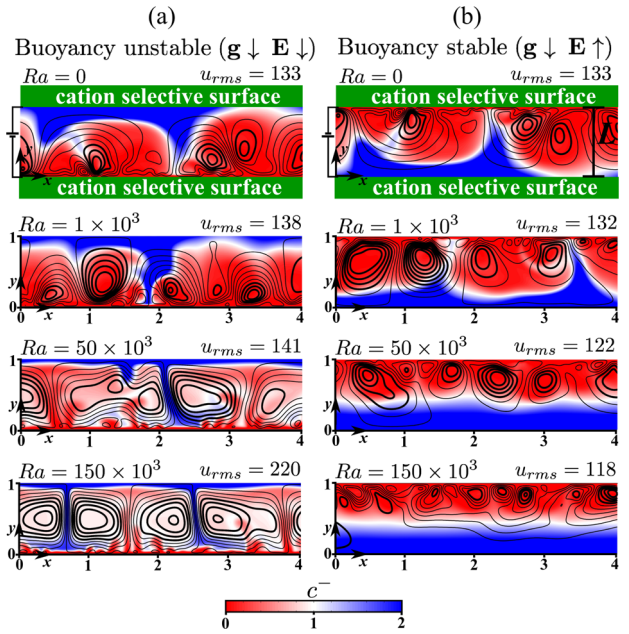

FIG. 1. Aqueous monovalent salt solution between two horizontal cation-selective surfaces subject to dc electric field in a gravitationally (a) unstable and (b) stable arrangement. Surface plots show the fully developed anion-concentration fields at $t = 0.2$ superimposed with flow streamlines. Here, $\Delta\phi = 80V_T$, $\kappa = 0.5$. The u_{rms} is scaled by D/L.

Despite decades of research revealing the significance of gravitational convection as well as electrokinetic instabilities in electrochemical systems, a quantitative understanding of coupling between these effects is not yet developed. In this Letter, we thoroughly examine the interplay of gravitational convection and chaotic electroconvection via 2D direct numerical simulations (DNSs).

We consider an aqueous solution of a univalent salt in between two horizontal cation-selective surfaces at $y = 0$ and $y = 1$ (Fig. 1). The fluid electrolyte is initially at a quiescent state with a uniform bulk concentration c_b. Incompressible Navier-Stokes and Poisson-Nernst-Planck equations describe the flow, electric potential, and ion transport, respectively:

$$\frac{1}{Sc}\left[\frac{\partial \boldsymbol{u}}{\partial t} + \boldsymbol{u}\cdot\nabla\boldsymbol{u}\right] = -\nabla p' + \nabla^2\boldsymbol{u} + \boldsymbol{f_e} + \boldsymbol{f_g}, \quad (1a)$$

$$\nabla\cdot\boldsymbol{u} = 0, \quad (1b)$$

$$-2\epsilon^2\nabla^2\phi = \rho_e, \quad (1c)$$

$$\frac{\partial c^{\pm}}{\partial t} = -\nabla\boldsymbol{j}^{\pm}. \quad (1d)$$

Here, $\boldsymbol{u} = u\hat{\boldsymbol{x}} + v\hat{\boldsymbol{y}}$ is the velocity vector field, p' is the modified pressure including the hydrostatic effects, c^+ is the cation concentration, c^- is the anion concentration, ϕ is the electric potential, and $\rho_e = z(c^+ - c^-)$ is the free charge density with ionic valence $z = \pm 1$. $\boldsymbol{f_e} = -\kappa\rho_e\nabla\phi/2\epsilon^2$ is the electrostatic body force, and $\boldsymbol{f_g} = -\hat{\boldsymbol{y}}c\mathrm{Ra}$ is the gravitational body force where $c = (c^+ + c^-)/2$ is the salt concentration. $\boldsymbol{j}^{\pm} = c^{\pm}\boldsymbol{u} - \nabla c^{\pm} \mp c^{\pm}\nabla\phi$ are ion fluxes of anions and cations. Equations (1a)–(1d) are dimensionless where the spatial coordinates, velocity, time, concentrations, and electric potential are respectively scaled by domain height L, diffusion velocity D/L, diffusion time L^2/D, bulk concentration c_b, and thermal voltage $V_T = k_BT/ze$, where k_B is the Boltzmann constant and e is the elementary charge.

In the Navier-Stokes equations [Eq. (1a)], we neglect the nonlinear terms $\boldsymbol{u}\cdot\nabla\boldsymbol{u}$ [11] and we employ the Oberbeck-Boussinesq approximation [34] in which the fluid density ρ is assumed to be a linear function of the salt concentration c; $\rho(c) = \rho_o[1 + \beta(c - c_b)]$, where ρ_o is the density of the fluid when $c = c_b$. Within the Oberbeck-Boussinesq approximation, the key dimensionless control parameters of our model problem are (i) the Rayleigh number $\mathrm{Ra} = \beta c_b g L^3/\nu D$, (ii) the electrohydrodynamic coupling constant $\kappa = \varepsilon V_T^2/(\nu\rho_o D)$ where ε is the dielectric permittivity, (iii) the dimensionless Debye length $\epsilon = \lambda_D/L$ where $\lambda_D = \sqrt{\varepsilon k_BT/[2(ze)^2c_b]}$ is the dimensional Debye length, and (iv) the dimensionless applied potential $\Delta\phi$ in units of thermal voltage. In our nondimensionalization, the Ra number is defined in terms of the initial bulk salt concentration c_b, instead of Δc, since in the overlimiting regime, the scale for the variation in the concentration Δc is $\mathcal{O}(c_b)$. We note that this is unlike the thermal RB problem where ΔT is the controlling parameter. Equations (1a)–(1d) are solved in a 2D domain, where periodic boundary conditions are implemented in the x direction over an aspect ratio of 6. No-slip boundary conditions are implemented along the cation-selective surfaces at $y = 0$ and $y = 1$. Zero-flux conditions are enforced for anions $\boldsymbol{j}^- = 0$ and dimensionless fixed cation concentration $c^+ = 2$ at $y = 0$ and $y = 1$. The gravity vector $\mathbf{g}$ points in the negative y direction. To explore both buoyantly unstable and stable systems, we consider different cases with difference in downward versus upward direction of the applied electric field (Fig. 1). We solve the governing equations with second order finite differences, as explained in detail in Ref. [12]. We studied the dynamics of interplaying buoyancy and electrokinetic effects in experimentally relevant regimes corresponding to a wide range of Ra number ($0 \le \mathrm{Ra} \le 1 \times 10^7$), applied potential $\Delta\phi$ ($5V_T \le \Delta\phi \le 100V_T$), and electrohydrodynamic coupling constant κ ($0 \le \kappa \le 0.5$). In all practical settings, ϵ is very small, typically in the range of 10^{-5} to 10^{-3}. In our study we consider a fixed $\epsilon = 10^{-3}$, which is small enough to capture essential EKI dynamics in the small ϵ limit while allowing reasonable computational cost for our investigations in a wide range of parameters. Nevertheless, our inspections

shown in the Supplemental Material [35] reveal that the net ion transport rate has a weak dependency on ϵ which is negligible compared to the dependency on Ra number and applied potential $\Delta\phi$ in the presented settings.

Figure 1 shows the fully developed anion concentration c^- fields superimposed with the flow lines for varying Ra numbers in gravitationally unstable and stable orientations at a fixed $\Delta\phi = 80V_T$. The top panels of Figs. 1(a) and 1(b) do not include the buoyancy effects ($\mathrm{Ra} = 0$) and are identical except for the direction of the electric field $\boldsymbol{E}$. When the buoyancy effects are considered at $\mathrm{Ra} = 1 \times 10^3$, the root mean square of the velocity u_{rms} varies slightly for the gravitationally unstable and stable arrangements, although the concentration fields remain qualitatively similar. The significance of the value of $\mathrm{Ra} = 1 \times 10^3$ is that it is on the order of the critical Rayleigh number $\mathrm{Ra}_{\mathrm{cr}}$ in systems that are governed solely by buoyancy effects [22,28,34,36]. However, we demonstrate that for a coupled system, the EKI effects are dominant for $\mathrm{Ra} \sim \mathcal{O}(10^3)$ when the applied voltage is sufficiently high. In dimensional units, $\mathrm{Ra} = 1 \times 10^3$ corresponds to $c_b \sim 1$ mM for a dilute NaCl solution with a domain length scale of $L \gtrsim 1.4$ mm. This scenario corresponds to $\epsilon = 10^{-5}$. However, we note again that the weak sensitivity of current on ϵ allows us to analyze the gravitational effects at $\epsilon = 10^{-3}$.

When $\mathrm{Ra} \gtrsim 1 \times 10^3$, the ion distribution and flow fields for buoyantly unstable and stable configurations are tremendously different. In the unstable configuration [Fig. 1(a)], RB structures are clearly observed in the form of large scale plumes ($\sim L$) detaching from the boundary layers at the cation-selective surfaces. For a moderate Ra, e.g., 50×10^3, the electrokinetic chaos prevails even in the large scale RB plumes, whereas for a higher Ra, e.g., 150×10^3, the large scale plumes become regularized in the form of convection cells. Nevertheless, the small scale EKI vortices are sustained for all Ra [third and fourth panels of Fig. 1(a)], even up to $\mathrm{Ra} \sim \mathcal{O}(10^6)$. This can be vividly seen by a comparison between top (EKI stable) and bottom (EKI unstable) membranes. Our investigations of a wide range of Ra numbers suggest that increasing Ra results in thinner, faster, and nearly regular cells consistent with the classical RB flows [34].

Figure 1(b) demonstrates gravitationally stable scenarios in which the ion-depleted layer is established near the top boundary. In this case, EKI vortices emerge at the upper membrane boundary. The domain partitions into two layers; in the lower layer, the EKI vortices are completely suppressed by the buoyancy effects and the transport is dominated by diffusion and electromigration. In the upper layer, while salt is highly depleted, there are still strongly active EKI vortices. In other words, buoyancy effects place an "edge" on the depth of penetration of EKI vortices. As the Ra number is increased, however, the edge of the upper layer is only slightly pushed back. Here, the mean salt concentration gradient is very small and associated with the so-called extended space charge layer [10]. The Δc over this zone, and thus the effective local Ra number, is much smaller than that of the nominal Ra number; thereby, the buoyancy forces cannot overcome the strong electrostatic body force due to EKI in this upper layer. In this case, the relative change in root-mean-square velocity $u_{\mathrm{rms}}/u_{\mathrm{rms}|_{\mathrm{Ra}=0}}$ remains $\approx\mathcal{O}(1)$, whereas in the gravitationally unstable configuration, $u_{\mathrm{rms}}/u_{\mathrm{rms}|_{\mathrm{Ra}=0}}$ can be as high as ≈ 15. We provide the plots of velocity, u_{rms}, free charge, energy, and concentration spectra, as well as movies in Ref. [35].

Next, we quantify the net transport rate in these systems by presenting the time and area averaged current density $\langle I \rangle$. In a gravitationally unstable arrangement when $\mathrm{Ra} \geq 1 \times 10^3$, the current density is higher for all $\Delta\phi$ compared to that for $\mathrm{Ra} = 0$ [Fig. 2(a)]. In addition, the characteristic plateau region, representing the diffusion limited transport, shortens for higher Ra number [Fig. 2(a)]. These observations are in a very good qualitative agreement with previous experimental reports [2–4,6,16,18]. The unstable RB plumes enhance the ion mass transfer by enhancing the fluid mixing, whereas in a gravitationally stabilized position, $\langle I \rangle$ diminishes and approaches a one-dimensional $\langle I \rangle$ sustained by only electromigration and diffusion. In this case, while EKI vortices are sustained in the upper layer, they do not substantially contribute to the net transport because they only cause mixing within a highly salt-depleted region.

In Fig. 2(b), we compare the instantaneous current I obtained at $\mathrm{Ra} = 0$ and $\mathrm{Ra} = 150 \times 10^3$ for the gravitationally unstable and stable configurations. The buoyancy forces damp the oscillations in I by regularizing the flow in both RB stable and unstable conditions. This observation also explains previous measurements in electrochemical

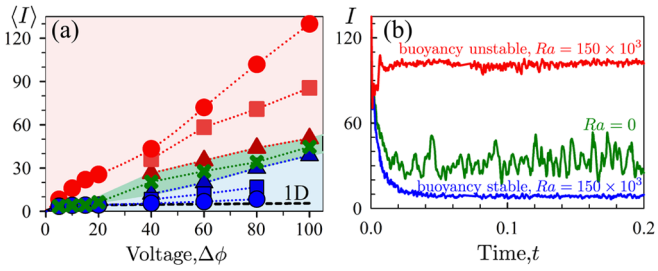

FIG. 2. Effect of magnitude and direction of the gravitational force. (a) Time averaged current density $\langle I \rangle$ where the cross symbols represent $\mathrm{Ra} = 0$ and the green shaded area depicts when gravitational effects are negligible. The red shaded area and the blue shaded area depict the gravitationally unstable and stable regimes, respectively. Triangles, squares, and circles represent $\mathrm{Ra} = 1 \times 10^3$, 50×10^3, and 150×10^3, respectively. The black dashed line presents the one-dimensional $\langle I \rangle$. (b) Instantaneous current density I at $\mathrm{Ra} = 0$ (green line) and $\mathrm{Ra} = 150 \times 10^3$ for gravitationally unstable (red line) and stable (blue line) configurations. Here, $\Delta\phi = 80V_T$. In (a) and (b), $\kappa = 0.5$.

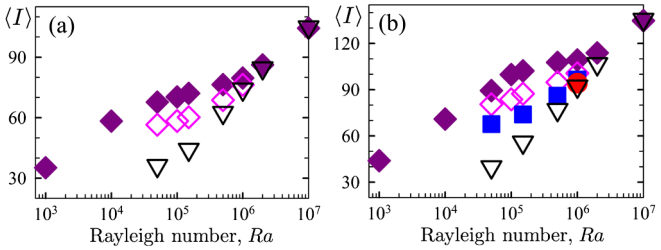

FIG. 3. Time averaged current density with respect to the Ra number obtained for gravitationally unstable configuration at (a) $\Delta\phi = 60V_T$ and (b) $\Delta\phi = 80V_T$ for various κ. In (a) and (b), $\kappa = 0.5$ (closed diamond), $\kappa = 0.2$ (open diamond), $\kappa = 0.1$ (square), $\kappa = 0.05$ (circle), and $\kappa = 0$ (downward triangle).

cells [2,22]. The amplitude of the oscillations is lower in the gravitationally stable position, whereas the oscillation period is similar for both configurations, determined by the frequency of EKI induced vortices thus by $\Delta\phi$ and κ at a given Ra number.

Our current density $\langle I\rangle$ results plotted with respect to Ra number (Fig. 3) imply the existence of an asymptotic convergence to a state in which ion mass transfer is dominated by gravitational effects. Figure 3(a) reveals that at a fixed $\Delta\phi = 60V_T$, and beyond $\mathrm{Ra} \approx 2 \times 10^6$, the current density becomes insensitive to κ. In this case, we even demonstrate for $\kappa = 0$, which signifies a hypothetical case of inactive EKI, the resulting current is close to that of finite κ. The asymptotic Ra number, however, depends on $\Delta\phi$ since it sets the base state. For a higher applied potential as in Fig. 3(b) ($\Delta\phi = 80V_T$), this asymptotic regime is reached at a higher $\mathrm{Ra} \approx 1 \times 10^7$. Our conclusion is that for the flow regimes relevant to electrochemical systems involving aqueous electrolytes, beyond the asymptotic Ra number on the order of 10^6 to 10^7, the EKI effects can be safely ignored.

To further investigate the lower Ra regime, in which EKI and RB are strongly coupled, we recast our numerical $\langle I\rangle$ data obtained for the gravitationally unstable orientation with power law fittings in the form of $\langle I\rangle = y_0 + m\mathrm{Ra}^n$ at each $\Delta\phi$ [Fig. 4(a)]. The intercept y_0 is supposedly the contribution of EKI to the current density, i.e., $I^{\mathrm{EKI}}|_{\mathrm{Ra}=0} = f(\Delta\phi, \kappa)$. Here, even for a constant $\kappa = 0.5$, the fitting parameters m and n are not constants but instead dependent on $\Delta\phi$ and κ, as opposed to the previous studies on electrochemical RB convection [19,20,22,29]. In these studies, n was reported to be a constant, often ~0.3 in agreement with the power law scalings reported for the thermal RB convection [37]. However, these previous correlations on electrochemical RB convection were obtained in the low voltage, diffusion limited regime and did not involve the EKI. Consistently, our results for $\kappa = 0$ indicate that the current shows a good power law correlation $m\mathrm{Ra}^{0.3}$ for all $\Delta\phi$ [Fig. 4(b)]. Here, the prefactors m vary with $\Delta\phi$ as the extent of initial density stratification, i.e., the extent of ion-concentration polarization, depends on the electric forcing $\Delta\phi$.

In the presented $\Delta\phi$, κ, and Ra number ranges, the EKI and RB instability do not linearly contribute to the total current density; thereby, for a given $\Delta\phi$ and κ, $\langle I\rangle \neq I^{\mathrm{RB}}|_{\kappa=0} + I^{\mathrm{EKI}}|_{\mathrm{Ra}=0}$. Instead, we propose the total current to be $\langle I\rangle(\kappa, \mathrm{Ra}, \Delta\phi) = I^{\mathrm{RB}}(\mathrm{Ra}, \Delta\phi)|_{\kappa=0} + I^*(\kappa, \mathrm{Ra}, \Delta\phi)$. Here, $I^* \neq I^{\mathrm{EKI}}|_{\mathrm{Ra}=0}$, but rather an additional current gained from the nonlinear coupling of EKI and RB convection. As seen in Fig. 4(c), I^* reveals a slow exponential decay with respect to Ra number for all κ. Here, we plot the regression lines $I^* = a \times e^{-b\mathrm{Ra}}$ obtained for $\Delta\phi = 80V_T$ for all κ where $a = f(\Delta\phi, \kappa)$ and $b = g(\Delta\phi, \kappa)$ are fitting parameters. Our regression analyses for $I^{\mathrm{RB}}|_{\kappa=0}$ and I^* show very good correlations for all κ and $\Delta\phi$ in the presented Ra number and $\Delta\phi$ ranges where both EKI induced vortices and RB plumes contribute to the total current. We attribute the absence of a universal fitting for m, a, and b to the highly nonlinear nature of the coupling between EKI and RB modes of flow.

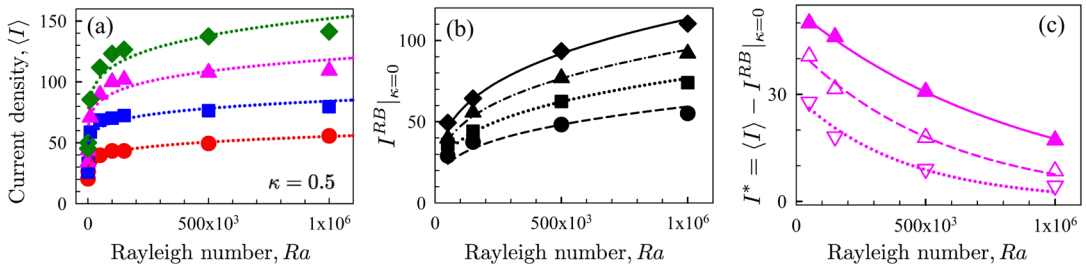

FIG. 4. Contributions of RB and EKI induced convection to the current density in a gravitationally unstable arrangement. (a) $\langle I\rangle$ data (symbols) plotted with a power law scaling $\langle I\rangle \sim y_0 + m\mathrm{Ra}^n$ (dotted lines) at a finite $\kappa = 0.5$ for various $\Delta\phi$, revealing poor correlations. (b) Current density data obtained at $\kappa = 0$ plotted with a power law scaling $\langle I\rangle(\kappa = 0) \sim \mathrm{Ra}^{0.3}$ for various $\Delta\phi$. (a),(b) $40V_T$, circles; $60V_T$, squares; $80V_T$, triangles; and $100V_T$, diamonds. (c) Current density I^* suggested to be induced by the chaotic EKI vortices with respect to Ra at $\Delta\phi = 80V_T$. The symbols present the DNS data obtained at $\kappa = 0.5$ (closed upward triangle), $\kappa = 0.2$ (open upward triangle), and $\kappa = 0.1$ (open downward triangle). Lines present exponential decay fits with respect to Ra; $I^* \sim e^{-b\mathrm{Ra}}$, where $b \sim \mathcal{O}(10^{-6})$ for $\kappa = 0.5$ (solid line), $\kappa = 0.2$ (dashed line), and $\kappa = 0.1$ (dotted line).

In summary, we have analyzed the buoyancy effects on electrokinetic chaos induced at ion-selective interfaces over a comprehensive range of parameters for the first time. Our results indicate that in the gravitationally stable scenario, buoyancy effects limit the growth of EKI vortices towards the buoyantly unstable ion-selective interface, while the EKI in the depleted layer remains strong. In the gravitationally unstable scenario, we demonstrated the interplay between two modes of mixing and quantified the asymptotic states in which the transport is dominated by either the EKI or RB mechanism. In practical scenarios, the quantified thresholds can be translated into system dimensions and experimental salt concentrations; thereby, they can provide significant guiding insights for the design and scaling analysis of a wide range of systems spanning from electrolytic applications such as electrodeposition and electroplating [30,33], energy conversion or storage such as batteries and supercapacitors, desalination systems [3,9], to even electro-osmotic pumps [38] in microfluidics.

The authors gratefully acknowledge Professor Andreas Acrivos for his invaluable comments on the manuscript and Scott Davidson for providing us with the parallelized DNS code. E. K. acknowledges the Rubicon grant from the Netherlands Scientific Organization NWO.

*karataye@gmail.com
†alimani@stanford.edu

[1] S. Nam, I. Cho, J. Heo, G. Lim, M. Z. Bazant, D. J. Moon, G. Y. Sung, and S. J. Kim, Phys. Rev. Lett. **114**, 114501 (2015).
[2] S. Lifson, B. Gavish, and S. Reich, Biophysics of Structure and Mechanism **4**, 53 (1978).
[3] J. Krol, J. Membr. Sci. **162**, 155 (1999).
[4] I. Rubinstein, E. Staude, and O. Kedem, Desalination **69**, 101 (1988).
[5] V. I. Zabolotsky, V. V. Nikonenko, N. D. Pismenskaya, E. V. Laktionov, M. Kh. Urtenov, H. Strathmann, M. Wessling, and G. H. Koops, Separat. Purificat. Technol. **14**, 255 (1998).
[6] N. Pismenskaia, P. Sistat, P. Huguet, V. Nikonenko, and G. Pourcelly, J. Membr. Sci. **228**, 65 (2004).
[7] S. M. Rubinstein, G. Manukyan, A. Staicu, I. Rubinstein, B. Zaltzman, R. G. H. Lammertink, F. Mugele, and M. Wessling, Phys. Rev. Lett. **101**, 236101 (2008).
[8] H.-C. Chang, G. Yossifon, and E. a. Demekhin, Annu. Rev. Fluid Mech. **44**, 401 (2012).
[9] J. C. de Valença, R. M. Wagterveld, R. G. H. Lammertink, and P. A. Tsai, Phys. Rev. E **92**, 031003(R) (2015).
[10] B. Zaltzman and I. Rubinstein, J. Fluid Mech. **579**, 173 (2007).
[11] C. L. Druzgalski, M. B. Andersen, and A. Mani, Phys. Fluids **25**, 110804 (2013).
[12] E. Karatay, C. L. Druzgalski, and A. Mani, J. Colloid Interface Sci. **446**, 67 (2015).
[13] S. M. Davidson, M. B. Andersen, and A. Mani, Phys. Rev. Lett. **112**, 128302 (2014).
[14] S. M. Davidson, M. Wessling, and A. Mani, Sci. Rep. **6**, 22505 (2016).
[15] V. V. Nikonenko, A. V. Kovalenko, M. K. Urtenov, N. D. Pismenskaya, J. Han, P. Sistat, and G. Pourcelly, Desalination **342**, 85 (2014).
[16] F. Maletzki, H.-W. Rosler, and E. Staude, J. Membr. Sci. **71**, 105 (1992).
[17] D. Deng, E. V. Dydek, J.-H. Han, S. Schlumpberger, A. Mani, B. Zaltzman, and M. Z. Bazant, Langmuir **29**, 16167 (2013).
[18] V. I. Zabolotsky, V. V. Nikonenko, and N. D. Pismenskaya, J. Membr. Sci. **119**, 171 (1996).
[19] C. R. Wilke, M. Eisenberg, and C. W. Tobias, J. Electrochem. Soc. **100**, 513 (1953).
[20] E. Fenech and C. Tobias, Electrochim. Acta **2**, 311 (1960).
[21] E. Hage and A. Tilgner, Phys. Fluids **22**, 076603 (2010).
[22] W. J. Ward and O. H. Le Blanc, Science **225**, 1471 (1984).
[23] G. Gonzalez, G. Marshall, F. Molina, and S. Dengra, Phys. Rev. E **65**, 051607 (2002).
[24] A. Pismenskiy, V. Nikonenko, M. Urtenov, and G. Pourcelly, Desalination **192**, 374 (2006).
[25] G. Marshall, E. Mocskos, G. Gonzalez, S. Dengra, F. Molina, and C. Iemmi, Electrochim. Acta **51**, 3058 (2006).
[26] S. Mühlenhoff, K. Eckert, A. Heinze, and M. Uhlemann, J. Electroanal. Chem. **611**, 241 (2007).
[27] J. R. de Bruyn, Phys. Rev. Lett. **74**, 4843 (1995).
[28] V. M. Volgin and A. D. Davydov, Russ. J. Electrochem. **42**, 567 (2006).
[29] R. J. Goldstein, H. D. Chiang, and D. L. See, J. Fluid Mech. **213**, 111 (1990).
[30] J. M. Huth, H. L. Swinney, W. D. McCormick, A. Kuhn, and F. Argoul, Phys. Rev. E **51**, 3444 (1995).
[31] A. Soba, G. Gonzalez, L. Calivar, and G. Marshall, Phys. Rev. E **86**, 051612 (2012).
[32] I. Winkler, I. Plevan, and V. Nechiporuk, Electrochim. Acta **41**, 2743 (1996).
[33] E. E. Mocskos, G. Gonzalez, F. V. Molina, and G. Marshall, J. Electroanal. Chem. **653**, 27 (2011).
[34] E. Koschmider, *Benard Cells and Taylor Vortices* (Cambridge University Press, Cambridge, England, 1993).
[35] See Supplemental Material at http://link.aps.org/supplemental/10.1103/PhysRevLett.116.194501 for additional plots of velocity, free charge, energy spectra, sensitivity of current density to nondimensional Debye length, and movies showing the evolution of anion concentration in gravitationally stable and unstable configurations.
[36] B. Baranowski and A. L. Kawczyński, Electrochim. Acta **17**, 695 (1972).
[37] G. Ahlers, S. Grossmann, and D. Lohse, Rev. Mod. Phys. **81**, 503 (2009).
[38] M. E. Suss, A. Mani, T. A. Zangle, and J. G. Santiago, Sens. Actuators A **165**, 310 (2011).